Article

Dynamic Equilibrium of a Supramolecular Dimeric Rhomboid and Trimeric Hexagon and Determination of Its Thermodynamic Constants

Takuya Yamamoto, Atta M. Arif, and Peter J. Stang

J. Am. Chem. Soc., **2003**, 125 (40), 12309-12317• DOI: 10.1021/ja0302984 • Publication Date (Web): 13 September 2003

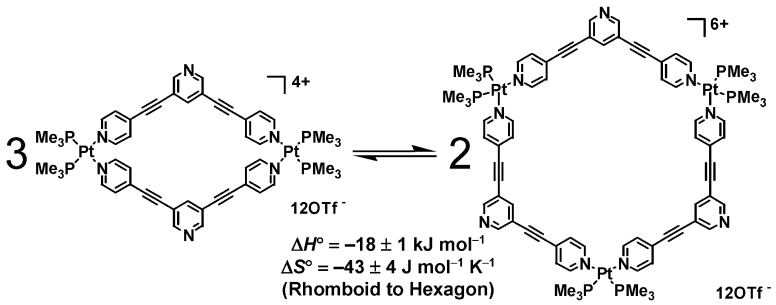

More About This Article

Additional resources and features associated with this article are available within the HTML version:

- Supporting Information
- Links to the 16 articles that cite this article, as of the time of this article download
- Access to high resolution figures
- Links to articles and content related to this article
- Copyright permission to reproduce figures and/or text from this article

View the Full Text HTML

J|A|C|S
ARTICLES
Published on Web 09/13/2003

Dynamic Equilibrium of a Supramolecular Dimeric Rhomboid and Trimeric Hexagon and Determination of Its Thermodynamic Constants

Takuya Yamamoto, Atta M. Arif, and Peter J. Stang*

Contribution from the Department of Chemistry, University of Utah, 315 South 1400 East, Salt Lake City, Utah 84112

Received May 19, 2003; E-mail: stang@chem.utah.edu

Abstract: A supramolecular dimeric rhomboid and its trimeric counterpart, a hexagon, are generated by design via the directional bonding methodology of self-assembly. The different-sized supramolecular macrocycles formed by Pt-coordination undergo a concentration- and temperature-dependent dynamic equilibrium. The two structures are characterized by multinuclear NMR and ESI-MS. Extensive study of the dynamic equilibrium of the two species in solution is performed to obtain its thermodynamic properties. By varying the ionic strength, μ, of the solutions, the *true* thermodynamic equilibrium constant, K, is determined at each experimental temperature ($K_{253} = 36 \pm 7$, $K_{273} = 18 \pm 6$, $K_{293} = 10 \pm 3$, $K_{313} = 9 \pm 2$, $K_{333} = 5 \pm 2$, and $K_{353} = 3.0 \pm 0.2$). By applying these values of *true K* at the respective temperatures to the van't Hoff equation extended with the entropy term, the standard enthalpy and entropy changes are determined for the equilibrium: with $\Delta H^\circ = -18 \pm 1$ kJ mol^{-1} and $\Delta S^\circ = -43 \pm 4$ J mol^{-1} K^{-1}, respectively, for the forward reaction (rhomboid to hexagon) of the equilibrium. The rhomboid is selectively crystallized, and its crystal structure is determined by X-ray diffraction. The structure reveals a significant amount of porosity as well as distortion of the rhomboid from planarity, leading to channels that can be observed from two viewing positions of the packing.

Introduction

The field of metal-directed supramolecular self-assembly by coordination chemistry has seen significant development for more than a decade.[1] Several studies have focused on equilibrating systems of supramolecular entities.[2] This field of chemistry has found practical applications in biological molecular recognition of receptor−substrates and mimics,[3] innovative dynamic materials,[4] and catalysis.[4b,5] Such systems rely on reversible association, which is often provided by labile metal−ligand coordination bonds, between basic components or precursors, spontaneously generating a supramolecular library of structures in dynamic equilibrium. Such dynamic molecular diversity, termed supramolecular polymorphism,[2a] ascribes to thermodynamic and kinetic parameters for the association of individual components. One of the most important concepts is to have multiple supramolecular entities in equilibrium, which have comparable free energies and exhibit a balanced distribution.[2a] This allows for a sensitive response to external stimuli and a tunable distribution of the desired products under given circumstances. In this sense, the dynamically equilibrating system possesses the inherent quality of self-decision for transforming itself according to the given information.[2c] Naturally, designing such dynamic equilibria and determining their physical properties are important for further development of the field. Studies of physical properties, including thermodynamics and kinetics,

(1) (a) Lehn, J.-M. *Supramolecular Chemistry-Concepts and Perspectives*; VCH: Weinheim, Germany, 1995. (b) Fujita, M.; Ibukuro, F.; Yamaguchi, K.; Ogura, K. *J. Am. Chem. Soc.* **1995**, *117*, 4175−4176. (c) Fujita, M.; Ibukuro, F.; Seki, H.; Kamo, O.; Imanari, M.; Ogura, K. *J. Am. Chem. Soc.* **1996**, *118*, 899−900. (d) Hartshorn, C. M.; Steel, P. J. *Inorg. Chem.* **1996**, *35*, 6902−6903. (e) Fujita, M.; Aoyagi, M.; Ibukuro, F.; Ogura, K.; Yamaguchi, K. *J. Am. Chem. Soc.* **1998**, *120*, 611−612. (f) Fujita, M. *Acc. Chem. Res.* **1999**, *32*, 53−61. (g) Sun, S.-S.; Lees, A. J. *J. Am. Chem. Soc.* **2000**, *122*, 8956−8967. (h) Cotton, F. A.; Lin, C.; Murillo, C. A. *Inorg. Chem.* **2001**, *40*, 472−477. (i) Sun, S.-S.; Anspach, J. A.; Lees, A. J. *Inorg. Chem.* **2002**, *41*, 1862−1869. (j) Cotton, F. A.; Daniels, L. M.; Lin, C.; Murillo, C. A. *J. Am. Chem. Soc.* **1999**, *121*, 4538−4539. (k) Sun, S.-S.; Lees, A. J. *Inorg. Chem.* **1999**, *38*, 4181−4182. (l) Navarro, J. A. R.; Lippert, B. *Coord. Chem. Rev.* **1999**, *185*−*186*, 653−667. (m) Cotton, F. A.; Lin, C.; Murillo, C. A. *Inorg. Chem.* **2001**, *40*, 575−577. (n) Fujita, M.; Yazaki, J.; Ogura, K. *Chem. Lett.* **1991**, 1031−1032. (o) Slone, R. V.; Benkstein, K. D.; Bélanger, S.; Hupp, J. T.; Guzei, I. A.; Rheingold, A. L. *Coord. Chem. Rev.* **1998**, *171*, 221−243. (p) Hasenknopf, B.; Lehn, J.-M.; Kneisel, B. O.; Baum, G.; Fenske, D. *Angew. Chem., Int. Ed. Engl.* **1996**, *35*, 1838−1840. (q) Hasenknopf, B.; Lehn, J.-M.; Boumediene, N.; Dupont-Gervais, A.; van Dorsselaer, A.; Kneisel, B.; Fenske, D. *J. Am. Chem. Soc.* **1997**, *119*, 10956−10962. (r) Noveron, J. C.; Lah, M. S.; Del Sesto, R. E.; Arif, A. M.; Miller, J. S.; Stang, P. J. *J. Am. Chem. Soc.* **2002**, *124*, 6613−6625. (s) Noveron, J. C.; Arif, A. M.; Stang, P. J. *Chem. Mater.* **2003**, *15*, 372−374.

(2) (a) Lehn, J.-M. *Chem.-Eur. J.* **1999**, *5*, 2455−2463. (b) Lehn, J.-M.; Eliseev, A. V. *Science* **2001**, *291*, 2331−2332. (c) Huc, I.; Lehn, J.-M. *Proc. Natl. Acad. Sci. U.S.A.* **1997**, *94*, 2106−2110.

(3) (a) Goodwin, J. T.; Lynn, D. G. *J. Am. Chem. Soc.* **1992**, *114*, 9197−9198. (b) Berl, V.; Huc, I.; Lehn, J.-M.; DeCian, A.; Fischer, J. *Eur. J. Org. Chem.* **1999**, 3089−3094. (c) Baxter, P. N. W.; Lehn, J.-M.; Rissanen, K. *J. Chem. Soc., Chem. Commun.* **1997**, 1323−1324. (d) Huc, I.; Krische, M. J.; Funeriu, D. P.; Lehn, J.-M. *Eur. J. Inorg. Chem.* **1999**, 1415−1420.

(4) (a) Liu, D. R.; Schultz, P. G. *Angew. Chem., Int. Ed.* **1999**, *38*, 36−54. (b) Maier, W. F. *Angew. Chem., Int. Ed.* **1999**, *38*, 1216−1218. (c) Lehn, J.-M. *Makromol. Chem., Macromol. Symp.* **1993**, *69*, 1−17. (d) Antonietti, M.; Heinz, S. *Nachr. Chem., Tech. Lab.* **1992**, *40*, 308−314. (e) Paleos, C. M.; Tsiourvas, D. *Angew. Chem., Int. Ed. Engl.* **1995**, *34*, 1696−1711. (f) Fernandez-Acebes, A.; Lehn, J.-M. *Adv. Mater.* **1999**, *11*, 910−913.

(5) (a) Hoveyda, A. *Chem. Biol.* **1998**, *5*, R187−R191. (b) Senkan, S. M.; Ozturk, S. *Angew. Chem., Int. Ed.* **1999**, *38*, 791−795. (c) Hill, C. L.; Zhang, X. *Nature* **1995**, *373*, 324−326. (d) Bein, T. *Angew. Chem., Int. Ed.* **1999**, *38*, 323−326.

have been common in supramolecular chemistry. For instance, such phenomena as association−dissociation,[6] conformational change,[7] and host−guest interaction[7b,8] were reported. Raymond and co-workers studied the activation parameters for supramolecular structural inversion and isomerization.[9] However, scarce research has been done on dynamic equilibria of supramolecular entities to obtain quantitative values for the thermodynamic parameters.

Several studies have encountered equilibrating supramolecular systems[10] including "unexpected" triangle−square equilibration from mixtures of 90° angular units and straight-side units.[10b−d,f,g,i−o] However, most of these studies were only qualitative in nature. The distribution of supramolecular entities in these equilibria was influenced by the addition of guest molecules as external stimuli,[10d,e] while others controlled the distribution by changing environmental conditions such as the concentration, temperature, and/or pressure.[10a,c−e,h,i,m−o] Although a certain number of reports generated supramolecular dynamic equilibria and successfully controlled the product ratio in a qualitative sense via enthalpic and entropic considerations, only two tentative studies have reported the quantitative thermodynamic properties (i.e., K, $\Delta H°$, and $\Delta S°$) of dynamic supramolecular equilibria.[10h,i] Thorough investigations are indispensable for the further development of a quantitative understanding of such equilibrating systems.

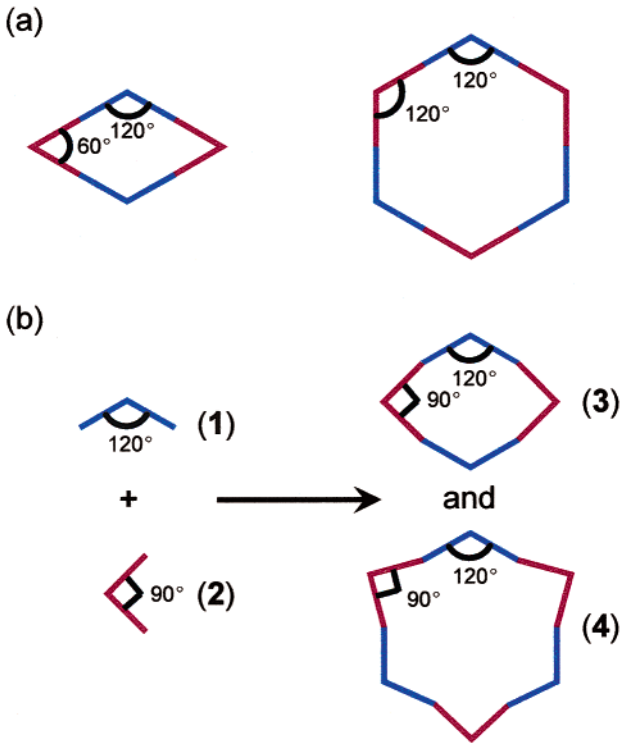

Figure 1. (a) Self-assembly of a supramolecular rhomboid (120° + 60°) and hexagon (120° + 120°) by the directional bonding approach. (b) Design of a rhomboid with convex sides (**3**) and a hexagon with concave sides (**4**) by using a 120°-angular unit (**1**) and a bisecting 90° complementary unit (**2**).

The blueprint for design of a dynamic equilibrium of metal-directed supramolecular entities was derived from conventional directional bonding methodology.[11] Herein, we report a predesigned dynamic equilibrium of supramolecular entities by using the bisecting angle, which is halfway between two theoretical angles required for two geometrically different macrocycles. A supramolecular rhomboid can result from the combination of two 120° and two 60° angles, while a supramolecular hexagon can be made from three 120° angular units reacting with another set of three 120° angular units by the directional bonding approach (Figure 1a). The pyridyl ligand 3,5-bis(4-pyridylethynyl)pyridine (**1**) plays the role of a 120° unit in both the rhomboid and the hexagon. This leaves 60° angles necessary for the assembly of the rhomboid. Another 120° tecton is necessary to complete the hexagon. By utilizing angular units, *cis*-$(Me_3P)_2Pt(OTf)_2$ (**2**),[10k,l,12] that are 90°, which bisects 60° and 120°, both the rhomboidal supramolecular structure with convex sides (**3**) and the hexagonal counterpart with concave sides (**4**) were expected as the outcome (Figure 1b). The convex and concave deviations from the ideal geometries were expected to be accommodated by the inherent flexibility in the acetylene-connected **1** and the angles of the pyridyl coordination to the Pt atoms. Moreover, when a labile coordination bond is employed, the system is expected to be under dynamic equilibrium. Herein, we report a quantitative study of the thermodynamics of the equilibrium to obtain K, $\Delta H°$, and $\Delta S°$, including consideration of the activity of the highly charged

(6) (a) Seto, C. T.; Whitesides, G. M. *J. Am. Chem. Soc.* **1993**, *115*, 1330−1340. (b) Wilcox, C. S.; Adrian, J. C., Jr.; Webb, T. H.; Zawacki, F. J. *J. Am. Chem. Soc.* **1992**, *114*, 10189−10197. (c) Jullien, L.; Cottet, H.; Hamelin, B.; Jardy, A. *J. Phys. Chem. B* **1999**, *103*, 10866−10875. (d) Fatin-Rouge, N.; Blanc, S.; Leize, E.; van Dorsselaer, A.; Baret, P.; Pierre, J.-L.; Albrecht-Gary, A.-M. *Inorg. Chem.* **2000**, *39*, 5771−5778. (e) Hanna, M. W.; Ashbaugh, A. L. *J. Phys. Chem.* **1964**, *68*, 811−816. (f) Yamamura, H.; Rekharsky, M.; Akasaki, A.; Araki, S.; Kawai, M.; Inoue, Y. *J. Phys. Org. Chem.* **2001**, *14*, 416−424.
(7) (a) Borovkov, V. V.; Lintuluoto, J. M.; Sugeta, H.; Fujiki, M.; Arakawa, R.; Inoue, Y. *J. Am. Chem. Soc.* **2002**, *124*, 2993−3006. (b) Xu, J.; Parac, T. N.; Raymond, K. N. *Angew. Chem., Int. Ed.* **1999**, *38*, 2878−2882.
(8) (a) Fujita, M. *Chem. Soc. Rev.* **1998**, *27*, 417−425. (b) Fujita, M.; Ogura, K. *Bull. Chem. Soc. Jpn.* **1996**, *69*, 1471−1482. (c) Fujita, M.; Nagao, S.; Iida, M.; Ogata, K.; Ogura, K. *J. Am. Chem. Soc.* **1993**, *115*, 1574−1576. (d) Fujita, M.; Yazaki, J.; Ogura, K. *J. Am. Chem. Soc.* **1990**, *112*, 5645−5647. (e) Shinkai, S.; Araki, K.; Manabe, O. *J. Am. Chem. Soc.* **1988**, *110*, 7214−7215. (f) Schneider, H.-J.; Rüdiger, V.; Raevsky, O. A. *J. Org. Chem.* **1993**, *58*, 3648−3653. (g) Bilyk, A.; Harding, M. M. *J. Chem. Soc., Chem. Commun.* **1995**, 1697−1698. (h) Mizyed, S.; Georghiou, P. E.; Ashram, M. *J. Chem. Soc., Perkin Trans. 2* **2000**, 277−280. (i) Yanase, M.; Matsuoka, M.; Tatsumi, Y.; Suzuki, M.; Iwamoto, H.; Haino, T.; Fukazawa, Y. *Tetrahedron Lett.* **2000**, *41*, 493−497. (j) Rekharsky, M.; Inoue, Y. *J. Am. Chem. Soc.* **2000**, *122*, 10949−10955. (k) Bhattacharya, S.; Nayak, S. K.; Chattopadhyay, S.; Banerjee, M.; Mukherjee, A. K. *J. Chem. Soc., Perkin Trans. 2* **2001**, 2292−2297.
(9) (a) Kersting, B.; Meyer, M.; Powers, R. E.; Raymond, K. N. *J. Am. Chem. Soc.* **1996**, *118*, 7221−7222. (b) Meyer, M.; Kersting, B.; Powers, R. E.; Raymond, K. N. *Inorg. Chem.* **1997**, *36*, 5179−5191. (c) Caulder, D. L.; Raymond, K. N. *J. Chem. Soc., Dalton Trans.* **1999**, 1185−1200. (d) Beissel, T.; Powers, R. E.; Parac, T. N.; Raymond, K. N. *J. Am. Chem. Soc.* **1999**, *121*, 4200−4206.
(10) (a) Fujita, M.; Aoyagi, M.; Ogura, K. *Inorg. Chim. Acta* **1996**, *246*, 53−57. (b) Romero, F. M.; Ziessel, R.; Dupont-Gervais, A.; van Dorsselaer, A. *J. Chem. Soc., Chem. Commun.* **1996**, 551−553. (c) Fujita, M.; Sasaki, O.; Mitsuhashi, T.; Fujita, T.; Yazaki, J.; Yamaguchi, K.; Ogura, K. *J. Chem. Soc., Chem. Commun.* **1996**, 1535−1536. (d) Lee, S. B.; Hwang, S.; Chung, D. S.; Yun, H.; Hong, J.-I. *Tetrahedron Lett.* **1998**, *39*, 873−876. (e) Ma, G.; Jung, Y. S.; Chung, D. S.; Hong, J.-I. *Tetrahedron Lett.* **1999**, *40*, 531−534. (f) Cotton, F. A.; Daniels, L. M.; Lin, C.; Murillo, C. A. *J. Am. Chem. Soc.* **1999**, *121*, 4538−4539. (g) Schnebeck, R.-D.; Freisinger, E.; Lippert, B. *Eur. J. Inorg. Chem.* **2000**, 1193−1200. (h) Mamula, O.; Monlien, F. J.; Porquet, A.; Hopfgartner, G.; Merbach, A. E.; von Zelewsky, A. *Chem.-Eur. J.* **2001**, *7*, 533−539. (i) Bark, T.; Düggeli, M.; Stoeckli-Evans, H.; von Zelewsky, A. *Angew. Chem., Int. Ed.* **2001**, *40*, 2848−2851. (j) Cotton, F. A.; Lin, C.; Murillo, C. A. *Acc. Chem. Res.* **2001**, *34*, 759−771. (k) Schweiger, M.; Seidel, S. R.; Arif, A. M.; Stang, P. J. *Angew. Chem., Int. Ed.* **2001**, *40*, 3467−3469. (l) Schweiger, M.; Seidel, S. R.; Arif, A. M.; Stang, P. J. *Inorg. Chem.* **2002**, *41*, 2556−2559. (m) Schalley, C. A.; Müller, T.; Linnartz, P.; Witt, M.; Schäfer, M.; Lützen, A. *Chem.-Eur. J.* **2002**, *8*, 3538−3551. (n) Sautter, A.; Schmid, D. G.; Jung, G.; Würthner, F. *J. Am. Chem. Soc.* **2001**, *123*, 5424−5430. (o) Fujita, M.; Ogura, K. *Coord. Chem. Rev.* **1996**, *148*, 249−264.
(11) (a) Stang, P. J.; Olenyuk, B. *Acc. Chem. Res.* **1997**, *30*, 502−518. (b) Stang, P. J. *Chem.-Eur. J.* **1998**, *4*, 19−27. (c) Leininger, S.; Olenyuk, B.; Stang, P. J. *Chem. Rev.* **2000**, *100*, 853−908.
(12) Leung, W.-H.; Chim, J. L. C.; Wong, W.-T. *J. Chem. Soc., Dalton Trans.* **1996**, 3153−3154.

Scheme 1

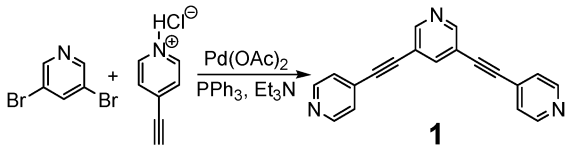

supramolecular entities.[13] Furthermore, an analysis of the porous packing of the crystal structure of **3**, which was selectively crystallized from the equilibrium, is reported.

Experimental Section

General. 3,5-Dibromopyridine and 4-ethynylpyridine hydrochloride were obtained from Aldrich and used without purification. All ambient and variable temperature NMR spectra were recorded on Varian Unity 300 or Varian XL-300 spectrometers. The ^{1}H NMR spectra were recorded at 300 MHz, and the chemical shifts were reported relative to the residual protons in the deuterated solvents, δ 7.27 and 4.33 ppm in $CDCl_3$ and CD_3NO_2, respectively. The $^{13}C\{^1H\}$ NMR spectra were recorded at 75 MHz, and the chemical shifts were reported relative to the ^{13}C in the deuterated solvents, δ 77.2 and 62.8 ppm in $CDCl_3$ and CD_3NO_2, respectively. The ^{19}F and $^{31}P\{^1H\}$ NMR spectra were recorded at 282 and 121 MHz, respectively, and the chemical shifts were reported relative to external standards of $CFCl_3$ and H_3PO_4, respectively, δ 0.0 ppm in each case. Uncorrected melting points were measured on a Laboratory Devices Mel-Temp instrument with an open capillary. The elemental analyses were carried out by Atlantic Microlab, Norcross, GA. EI-MS spectra were recorded on a Finnigan MAT 95 high-resolution gas chromatograph/mass spectrometer with a Finnigan MAT ICIS II operating system. ESI-MS spectra were recorded on a Micromass Quattro II triple quadrupole mass spectrometer with a Micromass MassLynx operating system.

3,5-Bis(4-pyridylethynyl)pyridine (1). Et_3N (7 mL) was added to a mixture of 3,5-dibromopyridine (999 mg, 4.21 mmol), 4-ethynylpyridine hydrochloride (1.50 g, 10.7 mmol; 2.5 equiv), palladium(II) acetate (98.8 mg, 0.440 mmol), and PPh_3 (223.2 mg, 0.851 mmol) (Scheme 1). The mixture was stirred and heated at 100 °C for 6 days under an N_2 atmosphere shielded from light. The resulting black material was suspended in CH_2Cl_2 (3.0 L) and washed with 3 portions of water. After the organic phase was dried over $MgSO_4$, it was filtered, and the solvent was removed in vacuo. The resulting black solid was taken up in acetone and $CHCl_3$ and filtered through a plug of silica gel. The filtrate was concentrated, and the residue was purified by column chromatography on silica gel, using acetone as eluent. Subsequent recrystallization from $CHCl_3$ via *n*-pentane diffusion gave off-white crystals of **1**. Yield: 366 mg (31%); mp 151−152 °C. ^{1}H NMR ($CDCl_3$): δ (ppm) 8.73 (d, J = 1.9 Hz, 2H, Py$H_{\alpha'}$), 8.63 (dd, J = 4.4, 1.5 Hz, 4H, PyH_α), 7.98 (t, J = 1.9 Hz, 1H, Py$H_{\gamma'}$), 7.38 (dd, J = 4.4, 1.5 Hz, 4H, PyH_β).[14] $^{13}C\{^1H\}$ NMR ($CDCl_3$): δ (ppm) 151.9, 150.1, 141.2, 130.4, 125.6, 119.3, 90.7, 89.2. EI-MS: *m*/*z* 280.9 (calcd for $[C_{19}H_{11}N_3]^+$ 281.1). Anal. Calcd for $C_{19}H_{11}N_3$: C, 81.12; H, 3.94; N, 14.94. Found: C, 80.62; H, 3.88; N, 14.70.

Rhomboid (3) and Hexagon (4). 3,5-Bis(4-pyridylethynyl)pyridine (**1**) (2.14 mg, 7.61 μmol) and *cis*-$(Me_3P)_2Pt(OTf)_2$ (**2**) (5.11 mg, 7.92 μmol) were mixed in CD_3NO_2 (2.0 mL) for 10 min at ambient temperature, resulting in a brown solution. NMR confirmed the existence of two different species. After filtration, the solvent was evaporated using a stream of dry N_2 gas, resulting in a brown solid, followed by washing with Et_2O. The mass spectra of **3** and **4** in acetone (ca. 1 mM) were determined by ESI-MS. Isolated yield: 6.29 mg (89%); mp 187−189 °C (dec). ^{1}H NMR (CD_3NO_2): δ (ppm) 8.92 (m, 12H, hexagon PyH_α), 8.88 (m, 8H, rhomboid PyH_α), 8.78 (d, J = 2.2 Hz, 6H, hexagon Py$H_{\alpha'}$), 8.74 (d, J = 2.2 Hz, 4H, rhomboid Py$H_{\alpha'}$), 8.13 (t, J = 2.0 Hz, 3H, hexagon Py$H_{\gamma'}$), 8.04 (t, J = 2.0 Hz, 2H, rhomboid Py$H_{\gamma'}$), 7.78 (bd, 12H, hexagon PyH_β), 7.73 (bd, 8H, rhomboid PyH_β), 1.76 (d, J_{H-P} = 11.2 Hz, 36H, rhomboid PC*H*), 1.70 (d, J_{H-P} = 11.5 Hz, 54H, hexagon PC*H*).[14] $^{13}C\{^1H\}$ NMR (CD_3NO_2): δ (ppm) 154.3, 152.9, 151.7, 151.6, 143.5, 143.3, 136.7, 136.6, 131.2, 131.2, 122.4 (q, J_{C-F} = 320 Hz, OTf), 119.6, 119.6, 95.3, 95.3, 89.7, 89.3, 14.6 (m), 14.5 (m). ^{19}F NMR (CD_3NO_2): δ (ppm) −80.[15] $^{31}P\{^1H\}$ NMR (CD_3NO_2): δ (ppm) −28.5 (s, J_{P-Pt} = 3149 Hz), −28.6 (s, J_{P-Pt} = 3149 Hz). ESI-MS: *m*/*z* 2630.4 (calcd for [**4** − OTf]$^+$ 2630.2), 1703.4 (calcd for [**3** − OTf]$^+$ 1703.1), 1240.5 (calcd for [**4** − 2OTf]$^{2+}$ 1240.6). Anal. Calcd for $(C_{27}H_{29}F_6N_3O_6P_2PtS_2)_2 \cdot CH_3NO_2 \cdot C_4H_{10}O$: C, 35.64; H, 3.60; N, 4.93; S, 6.45. Found: C, 35.95; H, 3.50; N, 4.97; S, 6.59.

Measurement of the Ratio of 3 to 4 in the Dynamic Equilibrium by NMR. Solid **3** and **4** (18.53 mg) were dissolved in 0.500 mL of CD_3NO_2 to form a solution with a component concentration[16] of 33.8 mmol kg^{-1}.[17] Successive dilution of the solution to prepare a series of component concentrations[16] of 30.4, 27.0, 23.7, 20.3, 16.9, 13.5, 10.1, 8.45, 6.76, 5.07, 3.63, 3.38, 2.11, 1.69, and 0.845 mmol kg^{-1} was performed. ^{1}H NMR spectra were recorded at each concentration to determine the ratio of **3** to **4** by integration of the signals from Py$H_{\gamma'}$.

For the variable temperature NMR experiments, the samples with the component concentrations[16] of 13.5, 8.45, 3.63, 2.11, and 0.845 mmol kg^{-1} were used. ^{1}H NMR spectra of these five concentrations were recorded at T = 253, 273, 293, 313, 333, and 353 K to determine the ratio of **3** to **4**. Standard CH_3OH and $HOCH_2CH_2OH$ samples, where applicable, were used to confirm the accuracy of the probe temperatures. Samples were allowed at least 20 min to equilibrate to the probe temperature. Although longer durations (up to 120 min) were allowed to elapse for a possible slow change in the **3** to **4** ratio, no significant changes were observed (i.e., the final ratio of **3** to **4** was achieved immediately after altering the concentration and/or temperature).

Analysis of the Data To Determine *True K*, $\Delta H°$, and $\Delta S°$. Three molecules of **3** with a 4+ charge each are in equilibrium with two molecules of **4** with a 6+ charge each; both sides of the equation are accompanied by 12 OTf^- counterions (Scheme 2). The *true* thermodynamic equilibrium constant (K) is defined as eq 1 where γ_i is the activity coefficient for the respective entities. The *apparent* equilibrium constant (K_{app}) is defined by the equilibrium quotient, which is the ratio of the supramolecular entities observed by NMR (eq 2). To reveal the *true K*, K_{app} must be determined where γ_i = 1, and then $K = K_{app}$ (eqs 1 and 2). The ionic strength, μ, which expresses the total concentration of ionic charges in solution, is defined as eq 3. The integral ratio of the NMR signals indicates the distribution of monomer units in **3** and **4**. The absolute concentration of each assembly was determined by multiplying these monomer ratios by the total monomer concentration (mol kg^{-1}), and then dividing by two for the rhomboid or three for the hexagon to correct for the stoichiometry. By substituting these absolute concentrations of **3** and **4** into eq 3, the ionic strengths of the solutions were obtained. The relationship of γ_i and μ can be expressed by the extended Debye−Hückel equation (eq 4), which works reasonably accurately when μ is less than 0.1 mol kg^{-1}.[18] When the ionic strength exceeds this value, it is known that the deviation from the equation

(13) Standard enthalpy and entropy changes of a solution-state reaction are defined at the concentration of 1 mol kg^{-1} (or 1 M) although each ionic species is assumed to behave as if in infinitely dilute solution (μ = 0 and γ_i = 1).

(14) PyH_α and PyH_β denote the hydrogen atoms of the terminal Py groups, whereas Py$H_{\alpha'}$ and Py$H_{\gamma'}$ denote the hydrogen atoms of the central Py group.

(15) ^{19}F NMR showed only a singlet, indicating that the exchange of the counterions OTf^- between the two supramolecular entities, **3** and **4**, is too fast to distinguish on the NMR time scale.

(16) Throughout the article, the "component concentration" of the solution with equilibrating **3** and **4** indicates the concentration of starting material **1** or **2** (monomer unit) for convenience of calculation.

(17) For the experiment involving a variety of temperatures, molality notation (mmol kg^{-1}) for the concentration expression is more accurate because varying the temperature changes the volume of the solvent, which then results in a change of the molarity concentration (mM).

(18) In the extended Debye−Hückel equation, A and B are constant, which are inherent to solvent at a given temperature, and a_i indicates the effective solvated radius of the ion.

Scheme 2

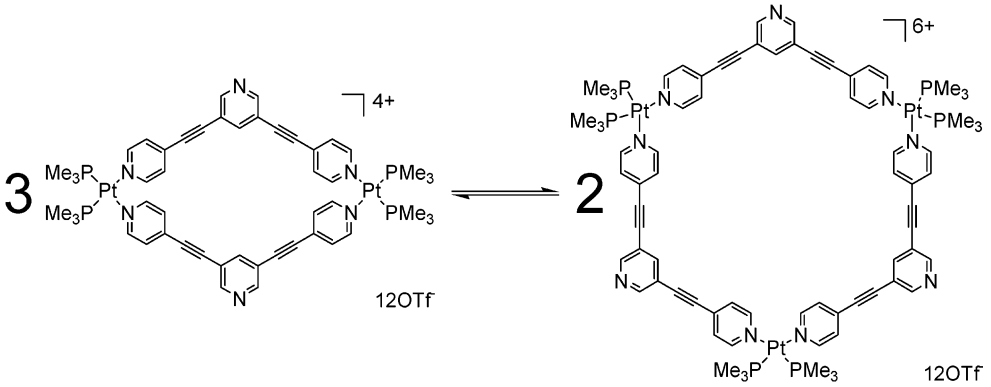

(**3**) (**4**)

can be significant by such factors as ion pair formation.[19] By definition, the activity coefficient, γ, approximates unity, when the solution is infinitely diluted; in other words, μ approaches zero. From eqs 1, 2, and 4, one can derive the new eq 5, where μ and K_{app} are the independent and dependent variables, respectively. A nonlinear regression of the K_{app} versus μ by the model eq 5 allowed us to determine the *true K*, which is equal to K_{app}, where $\mu = 0$, indicating imaginary zero-ionic strength (i.e., $\gamma \rightarrow 1$ and $K_{app} \rightarrow K$ as $\mu \rightarrow 0$).

$$K = \frac{[\text{hexagon}^{6+}]^2 \gamma^2_{\text{hexagon}^{6+}} [\text{OTf}^-]^{12} \gamma^{12}_{\text{OTf}^-}}{[\text{rhomboid}^{4+}]^3 \gamma^3_{\text{rhomboid}^{4+}} [\text{OTf}^-]^{12} \gamma^{12}_{\text{OTf}^-}} = \frac{[\text{hexagon}^{6+}]^2 \gamma^2_{\text{hexagon}^{6+}}}{[\text{rhomboid}^{4+}]^3 \gamma^3_{\text{rhomboid}^{4+}}} \quad (1)$$

$$K_{app} = \frac{[\text{hexagon}^{6+}]^2}{[\text{rhomboid}^{4+}]^3} \quad (2)$$

$$\mu = \frac{1}{2}\sum_i c_i z_i^2 = \frac{1}{2}\{[\text{rhomboid}^{4+}](+4)^2 + [\text{hexagon}^{6+}](+6)^2 + [\text{OTf}^-](-1)^2\} \quad (3)$$

$$\log \gamma_i = \frac{-Az_i^2\sqrt{\mu}}{1 + Ba_i\sqrt{\mu}} \quad (4)$$

$$K_{app} = K\frac{\left\{\exp\left(\frac{-Az^2_{\text{rhomboid}}\sqrt{\mu}}{1 + Ba_{\text{rhomboid}}\sqrt{\mu}}\right)\right\}^3}{\left\{\exp\left(\frac{-Az^2_{\text{hexagon}}\sqrt{\mu}}{1 + Ba_{\text{hexagon}}\sqrt{\mu}}\right)\right\}^2}, \quad \text{where } \exp(x) = 10^x \quad (5)$$

Because the *true K* value of the equilibrium is temperature dependent, a nonlinear regression was necessary for six series of K_{app} to determine the six *true K* values at the respective temperatures. The experimental K_{app} of the five sequential component concentrations[16] (0.845, 2.11, 3.63, 8.45, and 13.5 mmol kg^{-1}) was evaluated with a nonlinear regression treatment to provide the values of *true K* for the respective temperature series (see Results and Discussion).[20] The series of the six *true K* values at the temperatures were determined to be $K_{253} = 36 \pm 7$, $K_{273} = 18 \pm 6$, $K_{293} = 10 \pm 3$, $K_{313} = 9 \pm 2$, $K_{333} = 5 \pm 2$, and $K_{353} = 3.0 \pm 0.2$.[21] These *true K* values at the different temperatures were then used for the determination of the standard enthalpy and entropy changes of the forward (or backward) reaction in the equilibrium. The van't Hoff equation with the extension of the entropic term (eq 6),[22] which is derived from the two simultaneous equations of $\Delta G°$, was used to determine $\Delta H°$ and $\Delta S°$ for the equilibrium by the noncalorimetric method. The values of $-\ln K$[21] were plotted against $1/T$ to form the van't Hoff plot, in which $\Delta H°/R$ and $-\Delta S°/R$ are determined as the slope and the *y*-intercept, respectively, resulting in a reasonable linear plot where weighted least-squares were applied (see Results and Discussion). The linearity of the plot indicates the independence of $\Delta H°$ and $\Delta S°$ on temperature over the range by the definition of heat capacity at constant pressure, which is also applicable to the solution state.[23] By multiplying the values of the slope and the *y*-intercept by the gas constant, *R*, $\Delta H°$ and $\Delta S°$ for the equilibrium were obtained and found to be $\Delta H° = -18 \pm 1$ kJ mol^{-1} and $\Delta S° = -43 \pm 4$ J mol^{-1} K^{-1} for the forward reaction of **3** to **4**.[13]

$$-\ln K = \frac{\Delta H°}{R}\frac{1}{T} - \frac{\Delta S°}{R} \quad (6)$$

Results and Discussion

Synthesis of the 120° Angular Unit (1). The donor angular unit (**1**), which played the role of the 120° building block in the self-assembly, was synthesized by Sonogashira coupling of 3,5-dibromopyridine with 4-ethynylpyridine hydrochloride using palladium(II) acetate as the catalyst (Scheme 1).[24] It was characterized by ^{1}H and ^{13}C NMR, EI-MS, and elemental analysis. ^{1}H NMR shows the typical AA′BB′ splitting pattern for the terminal Py groups and an A_2B splitting pattern for the

(19) We determined that the experimental maximum component concentration[16] that was applicable to the extended Debye−Hückel was 13.5 mmol kg^{-1}, which gives an ionic strength of 0.0874 mol kg^{-1} at 253 K. Although we have obtained μ up to 0.220 mol kg^{-1} (33.8 mmol kg^{-1} by component concentration[16]) at the series of 293 K in the qualitative experiment, any data exceeding 0.1 mol kg^{-1} of ionic strength were not incorporated into the subsequent calculation.

(20) *Prism 3.03*; GraphPad Software Inc.: U.S., 2002.

(21) Because of the extrapolation of the nonlinear regression to $\mu = 0$, the values of *true K* were determined with relatively large fractional uncertainties, $\delta K_i/|K_i|$. However, the following conversion of *K* to $-\ln K$ reduced their propagated fractional uncertainties, $\delta(-\ln K_i)/|-\ln K_i|$, due to the nature of the logarithmic function. That is defined by propagation of uncertainty (i.e., if $q(x) = \ln x$, then $\delta q = \delta x|dq/dx| = \delta x|1/x|$). Values of $-\ln K$ with uncertainties at the experimental temperatures were determined to be $-\ln K_{253} = -3.6 \pm 0.2$, $-\ln K_{273} = -2.9 \pm 0.3$, $-\ln K_{293} = -2.3 \pm 0.3$, $-\ln K_{313} = -2.2 \pm 0.2$, $-\ln K_{333} = -1.5 \pm 0.4$, and $-\ln K_{353} = -1.11 \pm 0.07$.

(22) The van't Hoff equation is denoted by the derivative of the equation.

(23) Heat capacity at constant pressure (C_p) is defined by either enthalpy or entropy (i.e., $C_p = (\partial H/\partial T)_p = T(\partial S/\partial T)_p$). This equation can be expressed in ΔC_p. The linearity of the plot indicates $(\partial \Delta H/\partial T)_p = 0$ and the independence of ΔH on temperature over the range. The entropic expression of ΔC_p must be also equal to zero, $T(\partial \Delta S/\partial T)_p = 0$, and denotes that ΔS must be constant over the temperature range. Therefore, the slope of the plot simply represents $\Delta H°/R$, and the *y*-intercept corresponds to $-\Delta S°/R$.

(24) (a) Sonogashira, K.; Tohda, Y.; Hagihara, N. *Tetrahedron Lett.* **1975**, *16*, 4467−4470. (b) Sonogashira, K. *J. Organomet. Chem.* **2002**, *653*, 46−49. (c) Amoroso, A. J.; Thompson, A. M. W. C.; Maher, J. P.; McCleverty, J. A.; Ward, M. D. *Inorg. Chem.* **1995**, *34*, 4828−4835.

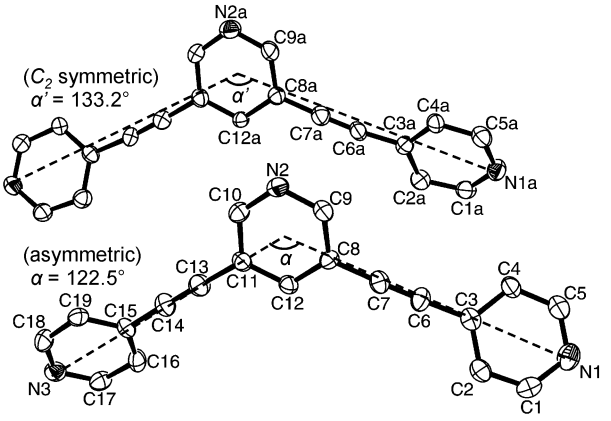

Figure 2. ORTEP representation of **1**. Hydrogen atoms are omitted for clarity. Thermal ellipsoids are drawn at 50% probability level. Two different conformations were observed; the top one possesses a C_2 axis, while the bottom is asymmetric.

central Py group. ^{13}C NMR shows six signals from the aromatic carbon atoms and two signals from the acetylenic carbon atoms. EI-MS shows the signal for the molecular ion with an unambiguous isotope distribution pattern well-matched to the calculated one. Furthermore, single crystals of **1** were obtained by diffusion of *n*-pentane into a $CHCl_3$ solution of **1**. X-ray diffraction of the single crystal revealed that the asymmetric unit of the compound contains 1.5 molecules so that **1** possesses two different conformations in its crystal structure, one asymmetric conformation and another conformation with C_2 symmetry, in which the angles of interest α and α′ are 122.5° and 133.2°, respectively (Figure 2). Although the angles in the solid state do not necessarily reflect those in solution, it can be deduced from these data that the "120°" unit has a certain degree of flexibility mostly due to the acetylene connectors. The flexibility is expected to accommodate the outward strain for the assembly of **3**, in which the sum of the theoretical angles of the four components exceeds the ideal 360° for a rhomboid, and the inward strain for the assembly of **4**, where the sum of the theoretical angles of the six components is less than the ideal 720° for a hexagon (Figure 1b). Relevant crystallographic data for **1** are listed in Table 1.

Self-Assembly of the Supramolecular Rhomboid (3) and Hexagon (4) in Dynamic Equilibrium. Simply mixing a one-to-one ratio of **1** and **2** in CD_3NO_2 generated the essentially instantaneous dynamic equilibrium of supramolecular entities **3** and **4**. Due to the D_{2h} symmetry of **3** and the D_{3h} symmetry of **4**, only two signals from each of PyH_α, PyH_β, Py$H_{\alpha'}$, Py$H_{\gamma'}$,[14] and PMe_3 were observed in the ^{1}H NMR spectra (i.e., all eight PyH_α in **3** are equivalent and appeared as one signal, which was distinguishable from another signal from the 12 equivalent PyH_α in **4**, and so forth). The ^{31}P NMR spectrum showed two overlapping but discernible peaks, one from the four equivalent phosphorus atoms in **3** and the other from the six equivalent phosphorus atoms in **4**, with approximately the same integral ratio as that of the ^{1}H NMR spectrum (Figure 3). The accompanying satellite peaks resulting from the ^{195}Pt coupling were not resolvable for each structure due to extensive line broadening. As with other Pt−Py self-assemblies,[8a,b,10k−o] the ^{31}P NMR spectrum showed a significant upfield-shift of 7.7 ppm,[25] while the chemical shifts of the PyH_α and PyH_β moved downfield by 0.25−0.29 and 0.22−0.27 ppm,[26] respectively, along with a noticeable broadening of the ^{1}H peaks upon complexation. The signals from the central Py (Py$H_{\alpha'}$, Py$H_{\gamma'}$) did not change significantly in terms of their chemical shifts, coupling constants, and peak widths from those of precursor **1** in the same solvent except for the complexation to form **3**, wherein Py$H_{\gamma'}$ shifted upfield by 0.09 ppm. The ^{1}H signal for PMe_3 shifted upfield by 0.09−0.15 ppm[26] from 1.85 ppm with a significant change in the splitting pattern. The ESI-MS spectra provided unambiguous evidence of the supramolecular entities, dimeric **3** and trimeric **4**, by the isotope distributions, which agreed with the calculated ones (Figure 4). Singly charged [**3** − OTf]$^+$ and [**4** − OTf]$^+$ have 1 amu of separation of the individual isotope peaks in the spectra, whereas the doubly charged [**4** − 2OTf]$^{2+}$ shows 0.5 amu of separation. No [**3** − 2OTf]$^{2+}$ or [**4** − 3OTf]$^{3+}$ were identified where a [**1** + **2** − OTf]$^+$ fragment appeared as a large signal at the same *m*/*z* number, which indicates that a noticeable degree of fragmentation also occurs under the conditions of ESI-MS. Analogous equilibria were observed by NMR in CD_3OD, CD_3CN, and acetone-d_6, showing solvent dependence. Similar self-assembly by reacting **1** with *cis*-$(Et_3P)_2Pt(OTf)_2$ also generated two species.

It is noteworthy that the central Py of **1** did not show any trace of reaction with **2** under this ratio of the precursors; only quantitative self-assemblies of **3** and **4** were observed. When more equivalents of **2** were used to force the central Py to coordinate to Pt, such as a two-to-three ratio of **1** and **2**, oligomerization was observed; both the ^{1}H and the ^{31}P NMR showed complex spectra with numerous overlapping peaks. The central Py appeared to be partially coordinated to the excess Pt

Table 1. Crystallographic Data for **1** and **3**

	1	**3**
empirical formula	$C_{19}H_{11}N_3$	$C_{55}H_{62}F_{12}N_6O_{13}P_4Pt_2S_4$
formula weight	281.31	1885.41
T (K)	150(1)	150(1)
wavelength (Å)	0.71073	0.71073
crystallographic system	monoclinic	triclinic
space group	*C*2	*P*1̄
unit cell dimensions		
a (Å)	34.5261(22)	8.6749(2)
b (Å)	6.0759(4)	9.0021(2)
c (Å)	10.5382(9)	23.7069(6)
α (deg)	90	92.2330(8)
β (deg)	101.6781(26)	97.2203(8)
γ (deg)	90	101.0409(16)
V (Å^3)	2164.9(3)	1798.87(7)
Z	6	1
density (Mg/m^3, calcd)	1.295	1.740
abs coeff (mm^{-1})	0.079	4.180
θ range for data collection (deg)	1.97−25.10	3.07−25.33
final *R* indices [$I > 2\sigma(I)$][a]		
R1	0.0663	0.0404
wR2	0.1400	0.1007
R indices (all data)		
R1	0.1101	0.0465
wR2	0.1582	0.1046

[a] $R1 = \sum(||F_o| - |F_c||)/\sum|F_o|$, $wR2 = [\sum(w(F_o^2 - F_c^2)^2)/\sum(F_o^2)^2]^{1/2}$.

(25) The line width of 5.3 Hz of the ^{31}P signal for the starting material *cis*-$(Me_3P)_2Pt(OTf)_2$, **2** (due to the complexation with H_2O), was reduced to 1.3 and 1.2 Hz for the dimer **3** and trimer **4** products upon assembly, respectively.

(26) The two hyphenated numbers indicate the chemical shift changes of the rhomboid-hexagon, respectively.

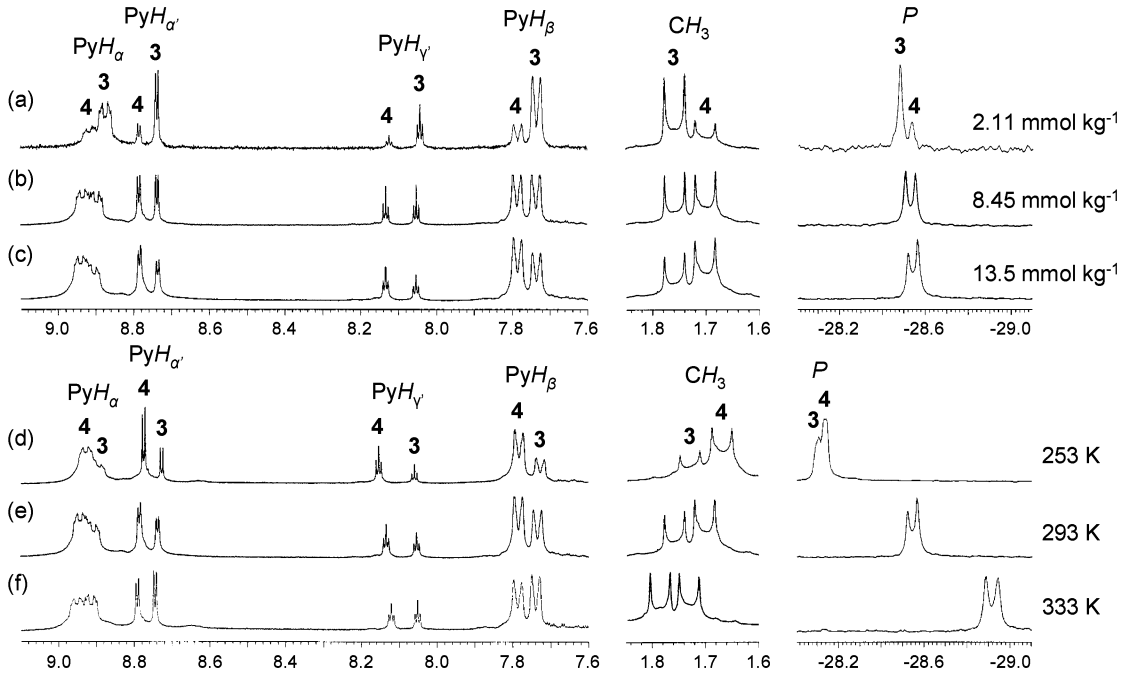

Figure 3. ^{1}H (left; aromatic region, middle; CH_3) and ^{31}P (right) NMR spectra of the dynamic equilibrium of **3** and **4**. (a−c) Concentration dependence of the equilibrium at constant temperature (293 K). (d−f) Temperature dependence of the equilibrium at constant component concentration[16] (13.5 mmol kg^{-1}).

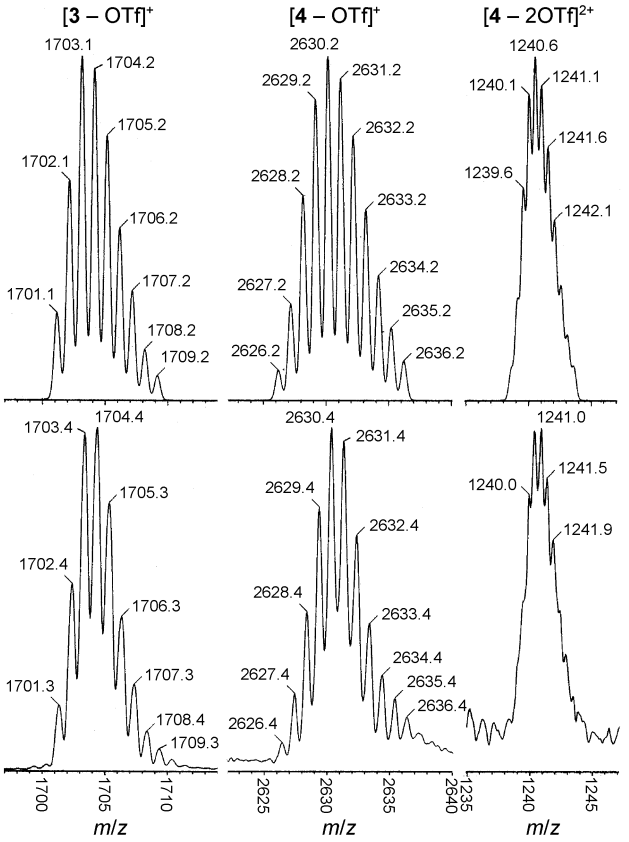

Figure 4. Calculated (top) and experimental (bottom) ESI-MS spectra of **3** and **4**.

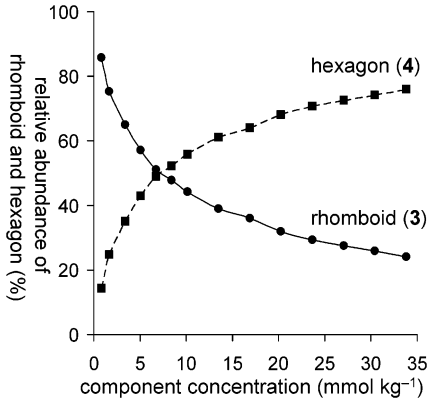

Figure 5. Relative abundance[27] of rhomboid (**3**) and hexagon (**4**) versus component concentration[16] at 293 K.

as ascertained by the chemical shifts and the integration of the ^{1}H NMR signals. The nitrogen atom of the central Py seems to have a much lower tendency to coordinate to Pt possibly due to steric and/or electronic factors. These oligomerized species could not be reassembled to any finite well-defined species by stirring them at elevated temperature up to 353 K.

NMR Experiments for the Qualitative Determination of Concentration and Temperature Dependencies. Several qualitative experiments on the relative abundance of assemblies in supramolecular equilibria have been reported, where NMR signals have been assigned to equilibrating species by concentration-dependent experiments.[10a,c−e,o] This is also applicable to the present case. The dimer, **3**, would be entropically favored over the trimer, **4**, because formation of **3** results in a greater number of particles than would that of **4**. This has a tendency to dominate at lower concentrations due to Le Châtelier's principle.

In NMR experiments of the equilibration of **3** and **4**, a similar dependence on concentration was observed. The aromatic signals of **3** resonated upfield relative to those of **4**. In contrast, the methyl and phosphorus signals of **3** were shifted downfield (Figure 3). A change in the integral ratio of **3** and **4**, as well as the chemical shifts, was observed by varying the concentration and temperature, indicating that the system was in dynamic equilibrium. The response (change of the signal ratio) to the internal (concentration) and the environmental (temperature)

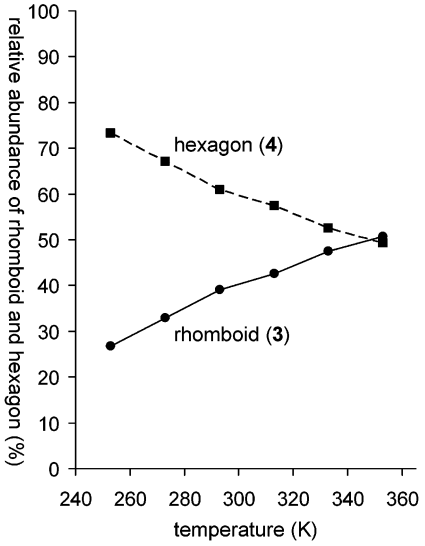

Figure 6. Relative abundance[27] of rhomboid (**3**) and hexagon (**4**) at constant component concentration[16] (13.5 mmol kg^{-1}) plotted against temperature.

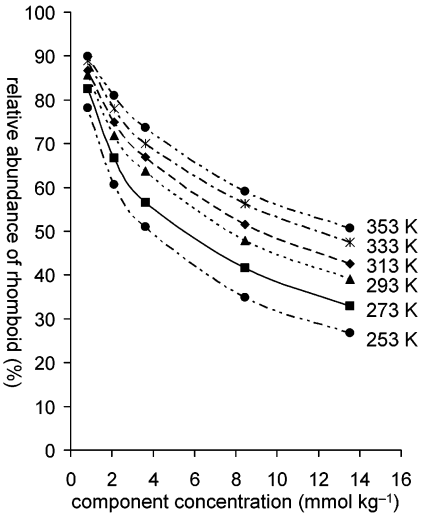

Figure 7. Relative abundance[27] curves of rhomboid (**3**) versus component concentration.[16] Each curve represents the relative abundance of **3** with respect to that of **4** at each temperature. Curves for hexagon (**4**) are omitted.

stimuli was essentially instantaneous in these experiments. In contrast, we have previously reported an equilibrating system that took an extended period to achieve the final ratio.[10l] It was observed that the proportion of **3** was increased with respect to that of **4** as the component concentration[16] decreased (Figure 3a−c) as well as when the temperature was increased (Figure 3d−f), and vice versa. The relative abundance[27] of **3** and **4** as a function of the component concentration[16] at constant temperature (293 K) is shown in Figure 5. The dimeric species **3** dominated at lower concentration. At the lowest experimental concentration (0.845 mmol kg^{-1}), which was near the lower detection limit of the NMR spectrometers, **3** had 85.8% relative abundance.[27] In contrast, the trimeric species **4** was favored at higher concentrations. At the highest experimental concentration (33.8 mmol kg^{-1}), **4** had a relative abundance[27] of 76.0%.

Moreover, as expected, the integral ratio of the signals was altered upon temperature change. The relative abundance[27] of

(27) "Relative abundance" denotes the ratio by NMR integration, which indicates the relative amount of the monomer unit consisting of **3** and **4**.

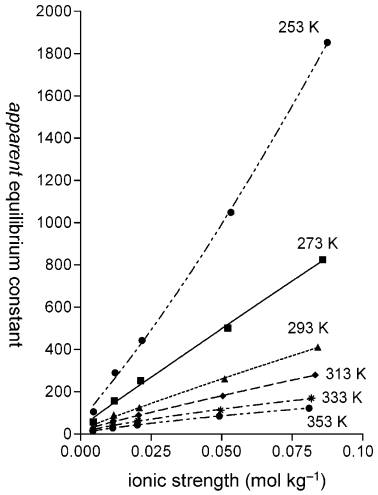

Figure 8. Plot of the *apparent* equilibrium constant (K_{app}) versus ionic strength (μ). A nonlinear regression was applied to each temperature series on the basis of the exponential function (eq 5).

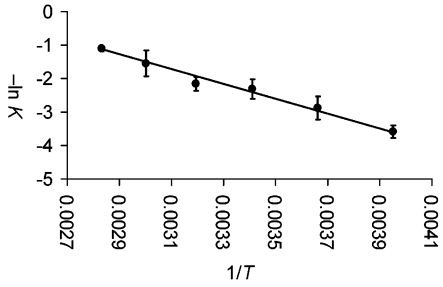

Figure 9. Van't Hoff plot for the equilibrium of **3** and **4**. Each point indicates the corresponding temperature series. The slope corresponds to the enthalpy term $\Delta H°/R$, and the y-intercept is equal to the value of $-\Delta S°/R$ (eq 6).

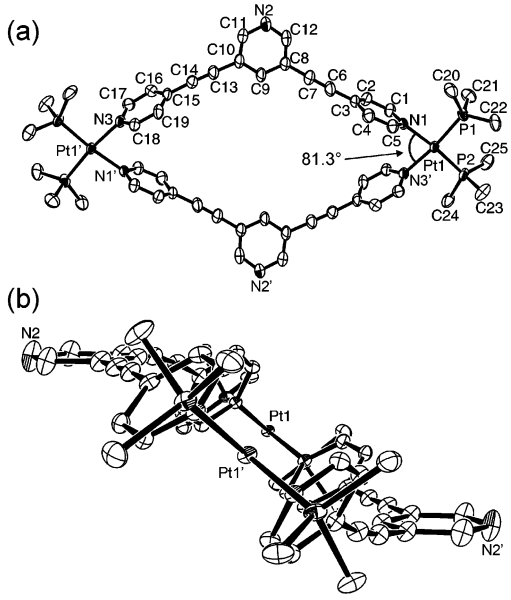

Figure 10. (a) Top view ORTEP representation of **3**. (b) Side view of the crystal structure model of **3** showing distortion from planarity. The structure possesses a C_2 axis. Hydrogen atoms, solvent molecules, and counterions are omitted for clarity. Thermal ellipsoids are drawn at 50% and 20% probability levels, respectively.

3 and **4** as a function of temperature with constant component concentration[16] (13.5 mmol kg^{-1}) is shown in Figure 6. The temperatures T = 253, 273, 293, 313, 333, and 353 K cover

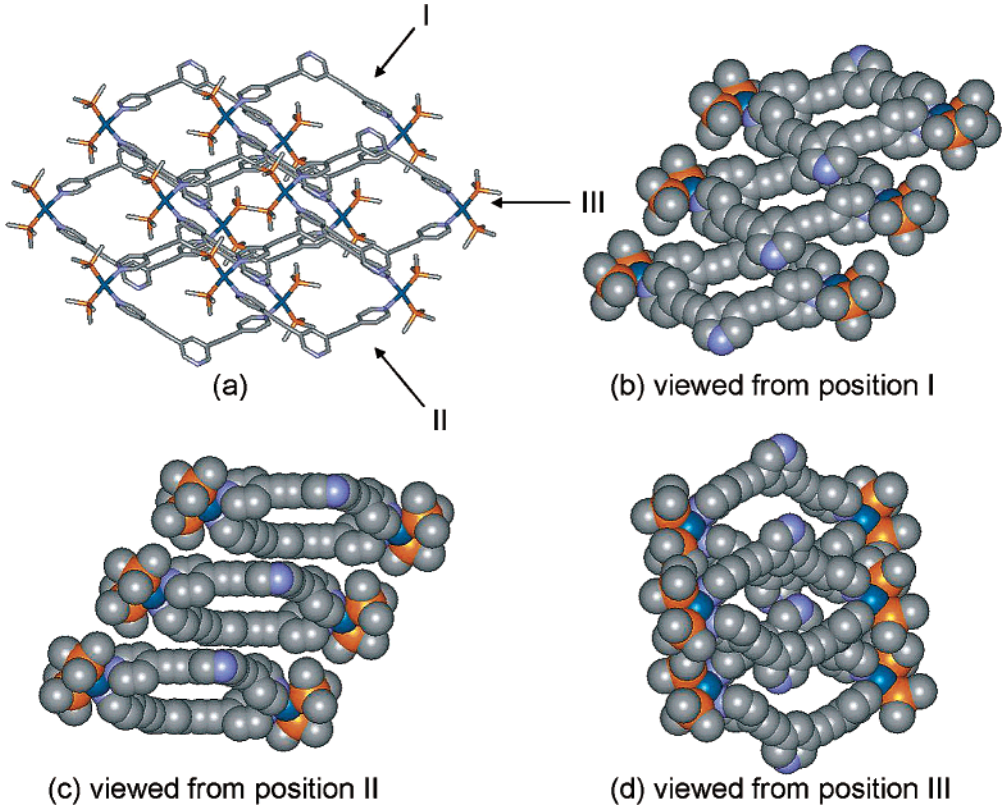

Figure 11. Packing diagrams of the crystal structure model of **3**. (a) Stick representation of the packing. Viewing positions I−III are shown. Hydrogen atoms, solvent molecules, and counterions are omitted for clarity. (b−d) CPK representations of the packing viewed from positions I−III, respectively.

the feasible experimental range of liquid CD_3NO_2. At a temperature of 253 K, **3** had a relative abundance[27] of 26.7%, while it increased to 50.7% when the temperature was raised to 353 K. This suggests, due to Le Châtelier's principle, the formation of **3** in the equilibrium is endothermic, or unfavorable in terms of enthalpy. Consequently, this dynamic equilibrium was based on the balance of entropically favorable **3** and enthalpically favorable **4**.

Study of the Concentration and Temperature Dependence of the Equilibrium and Determination of the Thermodynamic Constants. The quantitative determinations of $\Delta H°$ and $\Delta S°$ of supramolecular equilibria were first reported for systems consisting of Ag^+ and Zn^{2+}.[10h,i] Although these experiments were carried out without considering the activities of the ionic entities, the reports clearly pointed to the importance of obtaining $\Delta H°$ and $\Delta S°$ as numerical values.

The *true K* value at each experimental temperature, that accounts for the activity of the ionic entities, can be determined by applying a nonlinear regression of eq 5, which itself was derived from the equilibrium expressions (eqs 1 and 2) and the extended Debye−Hückel law (eq 4), to the series of *apparent K* values at various concentrations. Subsequently, applying the values of the *true K* at the experimental temperatures to the van't Hoff equation allowed for the quantitative determination of $\Delta H°$ and $\Delta S°$[13] (see Experimental Section).

Comprehensive NMR experiments to measure the ratio of **3** to **4** at the sequential component concentrations[16] (0.845, 2.11, 3.63, 8.45, and 13.5 mmol kg^{-1}) at each experimental temperature (T = 253, 273, 293, 313, 333, and 353 K) were carried out. The relative abundance[27] curves of **3** with respect to **4** are shown in Figure 7. Within the same temperature, the relative abundance[27] of **3** decreases as the component concentration[16] increases, which is comparable to the low-concentration portion ($\leq$ 13.5 mmol kg^{-1}) of the rhomboid curve in Figure 5. As seen for Figure 7, an increase in temperature results in an increase in **3** at any given component concentration.[16] When the data were converted to the plot of K_{app} versus μ, each temperature series formed a pseudolinear curve (Figure 8), although they are based on the exponential equation (eq 5). The "slope" of the curves became smaller with the temperature increments. By applying a nonlinear regression to this plot, the *true K* values were determined at each experimental temperature ($K_{253} = 36 \pm 7$, $K_{273} = 18 \pm 6$, $K_{293} = 10 \pm 3$, $K_{313} = 9 \pm 2$, $K_{333} = 5 \pm 2$, and $K_{353} = 3.0 \pm 0.2$). It is noteworthy that if the effect of γ_i were ignored, then an arbitrary value of K_{app} would be the *true K* value (eqs 1 and 2), where K_{app} would be independent of μ. This is clearly not the case and serves to illustrate the importance of considering γ_i. With the consideration of activity, the *true* values of *K* proved to be much smaller than K_{app} at any point of the respective temperature series; yet they still maintain the same tendency of becoming smaller with increased temperature. It is also noteworthy in the plot that, although the component concentration[16] is the same, the resulting ionic strengths (eq 3) were different at different temperatures because the ratios of **3** and **4** were temperature dependent.

The standard enthalpy and entropy changes, $\Delta H°$ and $\Delta S°$,[13] of the forward (or backward) reaction in the equilibrium were determined by applying the *true K* values[21] to the van't Hoff equation with the entropy term extension (eq 6)[22] utilizing weighted linear least-squares (Figure 9), resulting in values of $\Delta H° = -18 \pm 1$ kJ mol^{-1} and $\Delta S° = -43 \pm 4$ J mol^{-1} K^{-1}

for the forward reaction (**3** to **4**). As described qualitatively by Le Châtelier's principle above, the dimeric **3** is favored by the entropic factor, whereas the trimeric **4** is an enthalpic product, although both the entropy and the enthalpy factors were relatively small. Such a small standard enthalpy change can be explained by the similarity in the angle of the ring strain. Because the overall number of coordination bonds does not change between the equilibrating **3** and **4** (i.e., a total of 12 Pt−Py bonds on both sides of the equilibrium), the difference in ring strain can be considered as one of the most influential factors. In these macrocyclic molecules, **3** has an outward ring strain of 30° per monomer unit, while **4** has an inward ring strain of 30° per monomer unit (Figure 1b). Although the direction of the strain is opposite, the same amount of deviation from the theoretical angles exists in both supramolecular entities. Thus, only a small difference in $\Delta H°$ is expected.

Crystal Structure of Rhomboid (3). Although the system was in dynamic equilibrium, a single structure selectively crystallized from solution. By diffusing Et_2O into a methanol solution of the equilibrium, crystals of **3** were obtained (Figure 10). Pertinent crystallographic data for **3** are summarized in Table 1. A comparable crystal structure was also obtained by diffusion of Et_2O into an acetonitrile solution (**3b**). The rhomboidal structure of **3** has external dimensions of 23.9 × 12.7 Å, while the internal cavity of 17.7 × 7.7 Å embodies the porosity of the crystal. The N1−Pt1−N3′ angle, where the *cis*-Pt possesses a theoretical right angle, was 81.3°, showing the accommodation of the outward ring strain. Most of the remaining strain is presumably accommodated in the acetylene connected **1** and in the distortion of the rhomboidal structure from planarity (Figure 10b). The puckered structure causes an interesting packing (Figure 11). By stacking the entities along position I, the rhomboid cavities lie on top of each other and form one set of channels (Figure 11b). When the stacking diagram is viewed along position II, the cavities generated from the deviation from planarity of **3** (Figure 10b) overlap and form a different set of channels (Figure 11c). No channel is obvious from position III as it is obscured by the central Py rings of the adjacent rhomboids and OTf^- counterions (Figure 11d). One methanol molecule per macrocycle is observed inside the cavity.

Conclusion

Herein, we described the rapid dynamic equilibrium of a supramolecular rhomboid (**3**) and hexagon (**4**). ESI-MS confirmed the structures via isotope distributions. The NMR signals from **3** and **4** showed the concentration- and temperature-dependent equilibrium qualitatively where Le Châtelier's principle applies. The comprehensive study of the equilibrium allowed for the quantitative determination of the *true* thermodynamic equilibrium constants (K), $\Delta H° = -18 \pm 1$ kJ mol^{-1}, and $\Delta S° = -43 \pm 4$ J mol^{-1} K^{-1}. To the best of our knowledge, this work represents the first instance in which these values have been investigated for equilibria of supramolecular structures where such variables as ionic strength and activity coefficients have also been considered. Moreover, the crystal structure of **3** was obtained, showing an interesting porous structure consisting of two different sets of channels, which may have further implications in host−guest chemistry and materials science.

Acknowledgment. We thank Dr. S. R. Seidel and Dr. C. Addicott for assistance in the preparation of this manuscript, Dr. E. Rachlin for mass spectrometry, and Dr. J. C. Noveron for helpful suggestions and discussions. Financial support from the National Science Foundation (CHE-9818472) and the National Institutes of Health (5R01GM57052) is gratefully acknowledged.

Supporting Information Available: X-ray crystallographic data of **1**, **3**, and **3b** (CIF) and NMR spectra (^{1}H and ^{13}C{^{1}H}) of **1** (PDF). This material is available free of charge via the Internet at http://pubs.acs.org.

JA0302984